Journal of Molecular Liquids 298 (2020) 112033

Contents lists available at ScienceDirect

Journal of Molecular Liquids

journal homepage: www.elsevier.com/locate/molliq

A computational model for suspensions of motile micro-organisms in the flow of ferrofluid

S. Nadeem [g,h], Adel Alblawi [b], Noor Muhammad [a,c,*], Ibrahim M. Alarifi [d], Alibek Issakhov [e], M.T. Mustafa [f]

[a] Department of Mathematics, Quaid-I-Azam University 45320, Islamabad, 44000, Pakistan
[b] Mechanical Engineering Department, College of Engineering, Shaqra University, Dawadmi, P.O. 11911, Ar Riyadh, 11564, Saudi Arabia
[c] Department of Mathematics, Texas A&M University, College Station, TX, 77843, USA
[d] Department of Mechanical and Industrial Engineering, College of Engineering, Majmaah University, Al-Majmaah, 11952, Riydh, Saudi Arabia
[e] Al-Farabi Kazakh National University, Av. al-Farabi 71, 050040, Almaty, Kazakhstan
[f] Department of Mathematics, Statistics & Physics, Qatar University, Doha, 2713, Qatar
[g] Mathematics and its Applications in Life Sciences Research Group, Ton Duc Thang University, Ho Chi Minh City, Vietnam
[h] Faculty of Mathematics and Statistics, Ton Duc Thang University, Ho Chi Minh City, Vietnam

ARTICLE INFO

Article history:
Received 6 August 2019
Received in revised form 2 October 2019
Accepted 29 October 2019
Available online 9 November 2019

Keywords:
Ferromagnetic nanofluid
Bioconvection
Heat transfer

ABSTRACT

The performance of friction drag, heat transfer rate, and mass transfer is illustrated the in boundary layer flow region via density of motile microorganisms. Magnetic dipole in presence of Curie temperature and density of motile microorganisms plays important role in stabilizing and controlling the momentum and thermal boundary layers. In this direction, the characteristics of the magnetic dipole on the suspensions of motile microorganisms in the flow of ferrofluid are incorporated. Heat flux in the suspensions of motile microorganisms and at the surface is computed via Fourier's law of heat conduction. Characteristics of sundry physical parameter on the ferrohydrodynamic, thermal energy, mass transfer, and bioconvection are computed numerically and analytically. It is depicted that an enhancement in thermal Rayleigh number results in the reduction of friction drag, thereby enhances the heat transfer rate and Sherwood number at the surface, while the local density of motile microorganisms enhance for larger values of bioconvection Lewis number. Further, it is characterized that bioconvection Rayleigh number has increasing behavior on the heat transfer in the boundary layer. Comparison with available results are found in an excellent agreement.

1. Introduction

The swimming orientation of a single cell or motile micro-organism is governed by the advection (due to bulk fluid motion) and the action of its flagella. The trajectory concerning its swimming velocity comparative to the working liquid can be influenced by several exterior components including gravity, rate of strain, nutrient concentration and vorticity of the fluid. For example, the trajectory of cells to swim up or down a chemically reactive fluid flow is termed as chemotaxis. Bacterial micro-organisms, for example, *Escherichia coli* and Bacillus subtilis swim by means of rotating flagella pushed with the aid of reversible motors inserted in the cell wall. The movements of these microorganisms can be depicted by run intervals which the cells swim around a straight line, scattered with tumbles during which the living micro-organism experiences arbitrary reorientation. Run intervals are a little bit longer when organism swim up or down a chemoattractant gradient [1].

Secondly, consider the bacteria, for example, the algal bacteria Chlamydomonas nivalis, which push themselves by playing out a breast-stroke with the help of their front flagella. These bottom substantial organisms tend to swim upwards because of the anisotropic mass circulation organelles inside their cell body. An upwards swimming inclination is named negative gravitaxis or negative geotaxis [2]. In the present analysis, the angle between the vertical direction and the axis of the cell relies on the rotational viscous drag and the distance between the center of mass and volume. Swimming focused by this system is named gyrotaxis [3].

Although in a suspension unaccompanied cells are separately guided by means of this exterior cues, their interactions are intervened through the liquids. Bioconvection, the common performance of a concentrated population of micro-organisms, leads to maintain, relatively time-varying or steady spatial patterns. For example, bioconvection happens when the upward-swimming organisms cause an unbalanced density stratification sufficiently extensive to trigger a Rayleigh-Taylor instability through dropping crest. In such a crest, the liquid speed beats the

* Corresponding author. Department of Mathematics, Quaid-I-Azam University 45320, Islamabad, 44000, Pakistan.
E-mail addresses: sohail.nadeem@tdtu.edu.vn (S. Nadeem), noor@math.tamu.edu (N. Muhammad).

https://doi.org/10.1016/j.molliq.2019.112033
0167-7322/

upward swimming speed of individual cells. In the beginning, the suspension is uniform, gradually upswimming happens due to the wellspring of oxygen at the upper surface. It should be kept in mind that the instabilities occur initially at the surface eventually cause downwelling plumes. These crest/plumes advect oxygen whole through the neighborhood [4–9]. Pedley et al. [10] considered a uniform suspension of gyrotatic cells and analyzed the growth of patterns of bioconvection. Raju et al. [11] studied the gyrotactic microbes in a radiative Casson fluid past a moving wedge. The impact of variable thermal conductivity and gravity effect on a gyrotactic microbes in a nanofluids were analyzed by Chamkha et al. [12]. Nield and Kuznetsov [13,14] deliberated the convection and bio-thermal convection in the flow of a viscous flow filled with microbes. Mosayebidorcheh et al. [15] scrutinized the characteristics of gyrotactic microbes and nanoparticles in the boundary layer flow. Abe et al. [16] depicted bioconvection in a capillary assay induced by chemotaxis bacteria. Xun et al. [17] analyzed the impacts of variable viscosity and thermal conductivity in the flow of a viscous fluid filled with gyrotactic microbes.

Ferrofluids are magnetic suspensions of ferrite nanoparticles suspended in a carrier liquid. In the present evaluation, the ferrite nanoparticles and motile microorganisms are suspended in the suspension of ferromagnetic nanofluid. Heat transfer in the flow of ferromagnetic nanofluids enhances in the presence of ferrite nanoparticles and motile microorganisms. In case of creeping flow (advective inertial forces are small compared with viscous forces), the presence of motile microorganisms in the flow of ferromagnetic nanofluid will enhance the friction drag and heat transfer rate at the surface. On the other hand, if the advective inertial forces are greater as compared with the viscous forces, the resulting drag friction will reduce and heat transfer rate will enhance, which is analyzed in the present analysis. Arrue et al. [18] studied the magnetic nanoparticles and reported its applications in drug delivery. Neuringer [19] analyzed the liquid flows in presence of magnetic and thermal gradient. Sivakumar et al. [20] discussed the radiative ferromagnetic fluid in presence of dissipation and partial slip over a heated surface. The engineers are interested in the enhancement of heat transfer rate and in the reduction of friction drag which is applicable to the electronic devices and other industrial and engineering applications [21–35].

The purpose of the analysis is to investigate theoretically the friction drag, heat transfer rate, mass transfer rate, and the density of motile microorganisms in the suspension of motile microorganisms. The analysis is carried out in the presence of Curie temperature and magnetic dipole. A comparison has been made in such a way that the axial velocity, temperature filed, concentration profile, and motile microorganisms density is analyzed in the presence and absence of bioconvection Rayleigh number. The constitutive equations of ferrohydrodynamics, thermal energy, concentration, and motile microorganisms are obtained in light of boundary layer assumption. Making use of appropriate similarity variables, the boundary value problem is solved via BVPh2-midpoint method and optimal homotopy analysis method (OHAM). The influence of sundry physical parameters on the suspension of motile microorganisms is incorporated via graphs and tables.

2. Ferrohydrodynamic, thermal energy, and bioconvection equations

2.1. Flow analysis

A horizontal layer occupied by a ferromagnetic suspension is taken in such a way that it contains both gyrotactic micro-organisms and ferrite nanoparticles. Fig. 1 shows the geometry of the analysis. The effect of the magnetic dipole is taken in such a way that its center exactly lies on the $y-$axis at a distance b from the $x-$axis. The magnetic field points of magnetic dipole are applied in positive $x-$direction. To make ferrofluid saturate, the magnetic dipole improve the magnetic field of significant strength. It is considered that the temperature at stretching

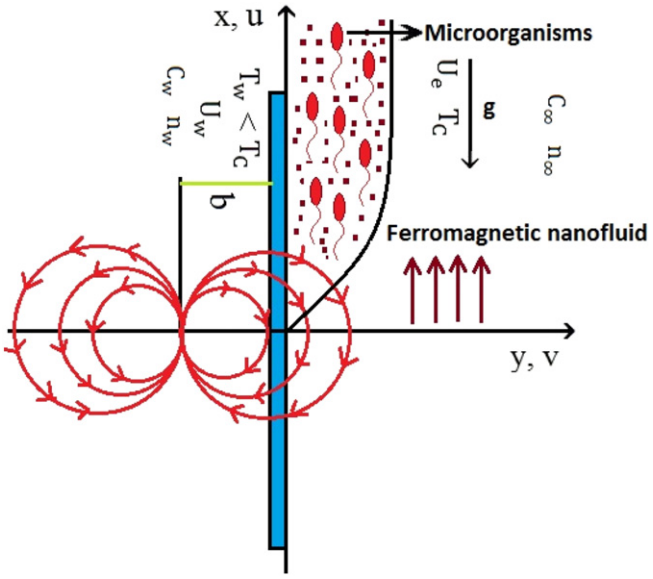

Fig. 1. Physical model.

surface T_w is less than the Curie temperature T_c, whereas, the temperature $T = T_\infty$ is presumed to be ambient temperature, i.e., $T_w<T_\infty<T_c$. The fluid above the Curie temperature T_c is not capable of being magnetized. Concerning nanoparticles, it is assumed that the nanoparticle suspension stay stable and they do not agglomerate in the flow of ferromagnetic nanofluid. In ferrofluid flow, it is consumed that the nanoparticles have no impact on their swimming velocity and on the direction of swimming of cells. The suspension of solid volume fraction nanoparticles is assumed to be diluted. This is due to the fact that bioconvection is possible in a dilute suspension. It is because of the comparison of suspension viscosity to the concentration of nanoparticles, if the viscosity becomes larger, the bioconvection suppressed [3]. Further, the analysis is carried out in presence of magnetic dipole, that is taken in such a way that its center lies on the $x-$axis at a distance b from the $x-$axis. The flow in the working fluid is induced by stretching of the sheet. The magnetic field points of magnetic dipole are taken along positive $x-$direction. The dimensionless governing boundary layer equations are given in Refs. [3,9,13]. The boundary layer equations in a ferrohydrodynamic, thermal energy, concentration, and microorganisms conservation equations are [14] directly defined as

$$\frac{\partial u}{\partial x}+\frac{\partial v}{\partial y}=0, \tag{1}$$

$$u\frac{\partial u}{\partial x}+v\frac{\partial u}{\partial y}-\frac{\mu_0 M\partial H}{\rho\ \partial x}=-\frac{1}{\rho_f}\frac{\partial P}{\partial x}+\upsilon\frac{\partial^2 u}{\partial y^2}+\frac{1}{\rho_f}\left((1-C_\infty)\rho_f\beta g(T-T_\infty)-\left(\rho_p-\rho_f\right)g(C-C_\infty)-(n-n_\infty)g\Delta\rho,\right. \tag{2}$$

$$u\frac{\partial T}{\partial x}+v\frac{\partial T}{\partial y}+\frac{\mu_0 T}{\rho}\left(u\frac{\partial H}{\partial x}+v\frac{\partial H}{\partial y}\right)\frac{\partial M}{\partial T}=\alpha_f\frac{\partial^2 T}{\partial y^2}+\tau\left(D_B\frac{\partial C\partial T}{\partial y\partial y}+\frac{D_T}{T_\infty}\frac{\partial T\partial T}{\partial y\partial y}\right). \tag{3}$$

$$u\frac{\partial C}{\partial x}+v\frac{\partial C}{\partial y}=D_B\frac{\partial^2 C}{\partial y^2}+\frac{D_T}{T_\infty}\frac{\partial^2 T}{\partial y^2}. \tag{4}$$

$$\frac{u\frac{\partial n}{\partial x}+v\frac{\partial n}{\partial y}+bW_cT}{(C_w-C_\infty)\frac{\partial}{\partial y}\left(n\frac{\partial C}{\partial y}\right)=D_m\frac{\partial^2 n}{\partial y^2}}. \tag{5}$$

The respective velocity components (u, v) are taken along $x-$ and $y-$ directions, μ signify viscosity of the suspension of microorganisms and ferromagnetic nanofluids, υ_f depicts the kinematic viscosity of ferrofluid, ρ_f signify base fluid density, the density of ferrite nanoparticles $\Delta\rho=\left(\rho_m-\rho_f\right)$ demonstrates the density difference between micro-organisms and base fluid, ρ_p denotes the density of the ferrite nanoparticle, P indicates pressure, β symbolizes volumetric thermal expansion coefficient of the base fluid, $\alpha_f=k/(\rho c_p)_f$ exhibits thermal diffusivity of the nanofluid, $(\rho c_p)_f$ discloses volumetric heat capacity of base fluid, whereas $(\rho c_p)_p$ volumetric heat capacity of nanoparticles, g indicates gravity, W_c is the maximum cell swimming speed, b is the chemotaxis constant, T symbolize the temperature of ferromagnetic nanofluid, C is the concentration, n is concentration of microorganisms, whereas, M expresses the magnetization, μ_0 exemplify the magnetic permeability, and H represents the magnetic field.

The admissible boundary conditions are assumed to be of the form

$$\begin{aligned}u|_y=0=U_w=ax,\ v|_y=0=0,\ T|_y=0=T_w, C|_y=0=C_w, n|_y\\ =0=n_w, u|_{y\to\infty}\to U_e=0,\ T|_{y\to\infty}\to T_\infty\\ =T_c\ C|_{y\to\infty}\to C_\infty\ n|_{y\to\infty}\to n_\infty\ .\end{aligned} \tag{6}$$

In above equations, U_w is the stretching velocity, a is the stretching rate, T_w, C_w, and n_w are the respective wall temperature, wall concentration of ferrite nanoparticles and surface concentration of microorganisms, T_∞, C_∞, and n_∞ are the respective ambient temperature, ambient concentration of ferrite nanoparticles and ambient concentration of microorganisms.

2.2. Magnetic dipole

The presence of magnetic dipole effects the ferrofluid flow due to its magnetic field. The magnetic field that effects the ferrofluid flow caused by magnetic dipole is illustrated by a magnetic scalar potential χ, where

$$\chi=\frac{\varrho}{2\pi}\frac{x}{x^2+(y+b)^2}, \tag{7}$$

here ϱ describes the magnetic field strength at the source. The components for the magnetic field H are

$$H_x=-\frac{\partial\chi}{\partial x}=\frac{\varrho}{2\pi}\frac{x^2-(y+b)^2}{\left(x^2+(y+b)^2\right)^2}, \tag{8}$$

$$H_y=-\frac{\partial\chi}{\partial y}=\frac{\varrho}{2\pi}\frac{2x(y+b)}{\left(x^2+(y+b)^2\right)^2}, \tag{9}$$

since the gradient of the magnetic of H is directly proportional to the magnetic body force, we thus have

$$H=\sqrt{\left(\frac{\partial\chi}{\partial x}\right)^2+\left(\frac{\partial\chi}{\partial y}\right)^2}. \tag{10}$$

Making use of Eqs. (8) and (9) in Eq. (10), and after expanded in powers of x and retained terms up to order x^2, we have the following expressions

$$\frac{\partial H}{\partial x}=-\frac{\varrho}{2\pi}\frac{2x}{(y+b)^4}, \tag{11}$$

$$\frac{\partial H}{\partial y}=\frac{\varrho}{2\pi}\left(\frac{4x^2}{(y+b)^5}-\frac{2}{(y+b)^3}\right), \tag{12}$$

the temperature and impact of magnetization M can be related in a linear way given below,

$$M=K(T-T_\infty), \tag{13}$$

here K exhibits the pyromagnetic co-efficient. The physical schematic of a heated ferrofluid is shown in Fig. 1, where the circular lines denote the magnetic field.

3. Solution procedure

Here we defined the similarity variables as considered by Andersson and Valnes [22].

$$\frac{\psi(\xi)=\left(\frac{a\mu}{\rho}\right)^{1/2}xf(\xi), \xi=y\left(\frac{\rho a}{\mu}\right)^{1/2}, \theta(\xi)=T-T_c}{\frac{T_w-T_c, \varphi(\xi)=\frac{C-C_\infty}{C_w-C_\infty}, j(\xi)=\frac{n-n_\infty}{n_w-n_\infty},}} \tag{14}$$

in which μ describes the dynamic viscosity and $\theta(\xi)$ exhibits dimensionless temperature, $\varphi(\xi)$ illustrates the dimensionless concentration, $j(\xi)$ shows the dimensionless microorganisms concentration, the stream function $\psi(\xi)$ are defined in such a way that the incompressibility condition (Eq. (1)) is directly satisfied, the comparable velocity components u and v are defined as follow

$$u=\frac{\partial\psi}{\partial y}=U_wf'(\xi),\ v=-\frac{\partial\psi}{\partial x}=-\sqrt{\frac{\mu a}{\rho}}f(\xi). \tag{15}$$

Using the similarity transformations given in Eqs. (14) and (15), the components of magnetic field due to magnetic field given in Eqs. (11) and (12) and magnetization M from Eq. (13) in Eqs. (2)–(5) along with the boundary conditions given in Eq. (6) reduces to the following boundary value problem

$$\frac{f''-f'2+ff''-2\beta_f\theta}{(\xi+r)^4+\lambda_b\theta-R_n\varphi-\frac{R_b}{L_b}j-R_m=0}, \tag{16}$$

$$\frac{\theta''+\mathrm{Pr}\ f\theta'+2\lambda\beta_f f(\theta-\varepsilon)}{(\xi+r)^3+N_b\theta'\varphi'+N_t\theta'2=0}, \tag{17}$$

$$\varphi''+Scf\varphi'+\frac{N_t}{N_b}\theta''=0, \tag{18}$$

$$j''+L_bfj'-P_e\left(\varphi''j+\varphi'j'\right)=0, \tag{19}$$

$$f(\xi)=0,\ f'(\xi)=1,\ \theta(\xi)=1,\ \varphi(\xi)=1,\ j(\xi)=1,\ \text{at}\ \xi=0, \tag{20}$$

$$f'(\xi)\to0,\ \theta(\xi)\to0,\ \varphi(\xi)\to0,\ j(\xi)\to0,\ \text{when}\ \xi\to\infty. \tag{21}$$

In the above boundary value problem the parameters λ_b (thermal Rayleigh number), R_m (basic-density Rayleigh number), R_b (bioconvection Rayleigh number), R_n (nanoparticle concentration Rayleigh number), β_f (ferrohydrodynamic interaction), λ (viscous dissipation), N_t (thermophoresis), ε (Curie temperature), N_b (Brownian motion), Sc (Schmidt number), Pr (Prandtl number), P_e (bioconvection

Peclet number), and L_b (bioconvection Lewis number) are defined as

$$\lambda_b = \frac{\rho_f \beta g(1-C_\infty)(T_w - T_c)}{\mu \alpha_f},\ R_n = \frac{g\left(\rho_p - \rho_f\right)(C_w - C_\infty)}{\mu \alpha_f},\ R_b = \frac{g\Delta\rho}{\mu D_m},\ N_b = \frac{\tau D_B (C_w - C_\infty)}{\alpha_f}, R_m = \frac{g\left(\rho_p n_w + \rho_f (1-n_w)\right)}{\mu \alpha_f},\ \varepsilon = \frac{T_c}{T_w - T_c},\ Sc = \frac{\upsilon_f}{D_B},\ \Pr = \frac{\upsilon_f}{\alpha_f},\ N_t = \frac{\tau D_T (T_w - T_c)}{\alpha_f T_c}, \beta_f = \frac{\varrho\, \mu_0 K (T_w - T_c)\rho_f}{2\pi \mu^2},\ \lambda = \frac{\mu^2}{\rho_f K (T_w - T_c)},\ \gamma = \sqrt{\frac{a\rho_f b^2}{\mu}},\ L_b = \frac{\alpha_f}{\upsilon_f D_m},\ P_e = \frac{bW_c}{D_m}. \tag{22}$$

Friction drag, local Nusselt number, Sherwood number, and the motile microorganisms density number are defined as

$$\frac{C_f = \frac{2\tau_w^{\,2}}{\rho U_w},\ Nu_x = \frac{x q_w}{k(T_w - T_c)},\ Sh_x = \frac{x\zeta_w}{D_B (C_W - C_\infty)},\ Nn_x = \frac{x j_w}{D_m (n_W - n_\infty)}}{} \tag{23}$$

where τ_w exhibits drag force at the wall, q_w identify heat flux at the surface, j_w signify mass flux at the surface, and the motile microorganisms density flux is symbolized by ζ_w, their mathematical expressions are

$$\tau_w = \mu \frac{\partial u}{\partial y}|_y = 0,\ q_w = -k\frac{\partial T}{\partial y}|_y = 0,\ \zeta_w = -D_B \frac{\partial C}{\partial y}|_y = 0,\ j_w = -D_m \frac{\partial n}{\partial y}|_y = 0. \tag{24}$$

Making use of Eqs. (23,24), the dimensionless form of friction drag, local Nusselt number, local Sherwood number, and the local motile microorganisms density are

$$\frac{1}{2}\mathrm{Re}^{1/2} C_f = f''(0),\ \mathrm{Re}^{-1/2} Nu_x = -\theta'(0),\ \mathrm{Re}^{-1/2} Sh_x = -\varphi'(0),\ \mathrm{Re}^{-1/2} Nn_x = -j'(0). \tag{25}$$

4. Optimal homotopy analysis method

The optimal homotopy analysis method (OHAM) [36,37] is described for the system of highly nonlinear problems emerging in nonlinear optimal control problems. The Optimal HAM contains convergence control parameters and is computationally rather productive. A sort of averaged residual error is characterized. The optimal convergence-control parameters is acquired to reduce the averaged residual error. The optimal HAM can be utilized to get quick convergent series solutions of various sorts of equations with strong nonlinearity. In present analysis, the boundary value problem is solved via optimal HAM. In optimal HAM, the non-linear equation can be reduced to a series of linear subproblems. It should be noted that initial guesses for the optimal problem can be produced utilizing a straightforward approach In light of just the initial boundary conditions. The established initial guesses and their relating linear operators for the boundary value problem are

$$L_f(f) = \frac{d^3 f^3}{d\xi} + \frac{d^2 f^2}{d\xi},\ L_\theta(\theta) = \frac{d^2\theta^2}{d\xi} - \theta, L_\varphi(\varphi) = \frac{d^2\varphi^2}{d\xi} - \varphi, L_j(j) = \frac{d^2 j^2}{d\xi} - j, \tag{26}$$

$$f_0(\xi) = 1 - \exp(-\xi),\ \theta_0 = \exp(-\xi),\ \varphi_0 = \exp(-\xi),\ j_0 = \exp(-\xi), \tag{27}$$

where $L_f(f)$, $L_\theta(\theta)$, $L_\varphi(\varphi)$ and $L_j(j)$ describes the linear operators, whereas $f_0(\xi)$, $\theta_0(\xi)$, $\varphi_0(\xi)$ and $j_0(\xi)$ illustrate the initial guesses of f, θ, φ and j respectively.

4.1. Convergence analysis

The convergence control auxiliary parameters h_f, h_θ, h_φ, and h_j are uses in optimal HAM to stabilize the convergence of homotopic solutions. The convergent solutions can be obtained by taking suggested values of these auxiliary parameters, these values can be calculated via optimal HAM. For this reason, residual square errors are noticed for momentum, energy and concentration equations by defining the expressions

$$\Delta_m^f = \int_0^1 [\mathcal{R}_m{}^f(\xi, h_f)]^2 d\xi, \tag{28}$$

$$\Delta_m^\theta = \int_0^1 [\mathcal{R}_m{}^\theta(\xi, h_\theta)]^2 d\xi, \tag{29}$$

$$\Delta_m^\varphi = \int_0^1 [\mathcal{R}_m{}^\varphi(\xi, h_\varphi)]^2 d\xi, \tag{30}$$

$$\Delta_m^j = \int_0^1 [\mathcal{R}_m{}^j(\xi, h_j)]^2 d\xi. \tag{31}$$

The convergence of the parametric values is displayed by optimal HAM, listed in the following Tables 1 and 2.

The graphical representation for the $12^t h$ order approximation displays the error decay in the Fig. 2.

Here Δ_m^t indicate the total discrete squared residual error.

$$\Delta_m^t = \Delta_m^f + \Delta_m^\theta + \Delta_m^\varphi + \Delta_m^n. \tag{32}$$

Here the Δ_m^t is used to obtain the optimal convergence control parameters.

5. Results and discussion

This paper predominantly talks about the impacts of the λ_b (thermal Rayleigh number), R_m (basic-density Rayleigh number), R_b (bioconvection Rayleigh number), R_n (nanoparticle concentration Rayleigh number), β_f (ferrohydrodynamic interaction), λ (viscous

Table 1
Shows average residual square errors (Δ_m^t).

Order	Values				
	$\hbar_f$	$\hbar_\theta$	$\hbar_\varphi$	$\hbar_j$	Δ_m^t
4	−0.115632	−0.326544	−0.732014	−0.210153	3.831×10^{-6}
6	−0.210801	−0.321669	−0.770312	−0.219810	4.5280×10^{-10}
8	−0.283174	−0.430212	−0.780431	−0.317801	7.6590×10^{-13}
10	−0.300130	−0.674320	−0.803217	−0.435011	2.3528×10^{-18}
12	−0.530621	−0.753901	−0.982001	−0.602170	5.0841×10^{-22}

Table 2
Shows individual residual square errors for $\Delta_m^f, \Delta_m^\theta, \Delta_m^\varphi$ and Δ_m^j.

order	values			
	$\hbar_f = -0.530621$	$\hbar_\theta = -0.753901$	$\hbar_\varphi = -0.982001$	$\hbar_j = -0.602170$
	Δ_m^f	Δ_m^θ	Δ_m^φ	Δ_m^j
6	4.45109×10^{-5}	6.71209×10^{-6}	4.00921×10^{-5}	6.76104×10^{-7}
10	2.08002×10^{-9}	9.77311×10^{-8}	7.43022×10^{-9}	8.66310×10^{-11}
18	8.99102×10^{-14}	8.55310×10^{-14}	8.93301×10^{-15}	4.88711×10^{-16}
24	1.99821×10^{-20}	5.03319×10^{-18}	3.44109×10^{-20}	5.08381×10^{-21}

dissipation), N_t (thermophoresis), ε (Curie temperature), N_b (Brownian motion), *Sc* (Schmidt number), Pr (Prandtl number), P_e (bioconvection Peclet number), and L_b (bioconvection Lewis number) on the axial velocity, temperature, concentration and density of motile microorganisms fields. The analysis is carried out for the case $\gamma = 1.0, \lambda = 0.01$, and $\varepsilon = 2.0$, whereas the values assigned to remaining parameters are as in Ref. [15]. Various physical parameters of engineering interest on the lower plate of the system, namely the local skin friction coefficient, Nusselt number, Sherwood number and wall motile microorganisms flux are also analyzed in detail. The boundary value problem is solved via numerical and analytical methods, i.e., the BVPh2−Midpoint method and the optimal HAM respectively. This section includes the physical interpretation of physical parameters on the flow field. The impacts of dimensionless submerging parameters λ_b (thermal Rayleigh number), R_m (basic-density Rayleigh number), R_b (bioconvection Rayleigh number), R_n (nanoparticle concentration Rayleigh number), β_f (ferrohydrodynamic interaction), λ (viscous dissipation), N_t (thermophoresis), ε (Curie temperature), N_b (Brownian motion), *Sc* (Schmidt number), Pr (Prandtl number), P_e (bioconvection Peclet number), and L_b (bioconvection Lewis number) are inspected. Moreover, rest of the materialize parameters in the flow of the boundary value problem are elevated fixed, i.e., $\gamma = 1.0, \lambda = 0.01$, and $\varepsilon = 2.0$.

The impacts of ferrohydrodynamic interaction parameter β_f on the axial velocity and temperature field are analyzed in Figs. 3 and 4. The presence of parameters γ (dimensionless distance from the center of magnetic dipole to the origin), β (ferrohydrodynamic interaction), and ε (Curie temperature) play a vital rule in holding the impact of ferromagnetic effect on the flow. The presence of ferrite (magnetite) nano sized particles in a carrier liquid correspond to ferrofluid, that leads to enhancing viscosity of the fluid, as a result, the axial velocity vanishes for larger values of parameter β_f (ferrohydrodynamic interaction) evident in Fig. 3. On the other hand, the impacts of β_f (ferrohydrodynamic interaction) on temperature field is depicted in Fig. 4. It is designated that temperature of the fluid is enhanced for larger values of parameter β_f (ferrohydrodynamic interaction). In fact, an increase in parameter β_f (ferrohydrodynamic interaction) leads to improve the interaction between ferrites nanoparticles of fluid and magnetic field action, which is responsible for enhancing frictional heat among fluid layers, as a result the thermal layer enhances.

The impacts of parameters R_m (basic-density Rayleigh number) and R_n (nanoparticle concentration Rayleigh number) on the axial velocity in the flow of bioconvection ferromagnetic nanofluid are designated in Figs. 5 and 6. It should be kept in mind that positive values of parameter R_n (nanoparticle concentration Rayleigh number) depicts the top-heavy ferrites nanoparticle layer. Therefore an enhancement in the R_n (nanoparticle concentration Rayleigh number) characterizes the destabilizing effect, as a result, the axial velocity reduces as shown in Fig. 5. An increase in R_m (basic-density Rayleigh number) leads to rising the viscosity of the fluid. Such enhancement in viscosity of fluids leads to enhance the interaction between ferrite nanoparticles and the magnetic field due to magnetic dipole. The resulting interaction causes reduction in motion among fluid layers, which is responsible for the reduction in axial velocity depicted in Fig. 6. Moreover, the impacts of parameters λ_b (thermal Rayleigh number) and R_b (bioconvection Rayleigh number) on the axial velocity in the flow of ferromagnetic fluid is carried out. It is incorporated that by giving variation to these two parameters leads to reduce the axial velocity shown in Figs. 7 and 8. If we take $R_b = 0$, it means that the suspension has no gyrotactic microorganisms, $R_b > 0$ corresponds to the case of upward-heavy (destabilizing) ferrite nanoparticle field, whereas, $R_b < 0$ bottom-heavy (stabilizing) ferrite nanoparticle profile. On the other hand, when $\lambda_b = 0$ it means that there is no heating in the suspension, $\lambda_b > 0$ depicts heating from the bottom, and $\lambda_b < 0$ corresponds to heating from top. In both the cases, we see that positive values of R_b (bioconvection Rayleigh number) leads heavy-upward ferrite nanoparticles distribution, which is responsible for the possible reduction in the axial velocity shown in Fig. 7. While, positive values of λ_b (thermal Rayleigh number) leads to heating from the bottom, which leads to enhancing the possible collision among ferrite nanoparticles and gyrotactic microorganisms, as a result the axial velocity thinning as shown in Fig. 8.

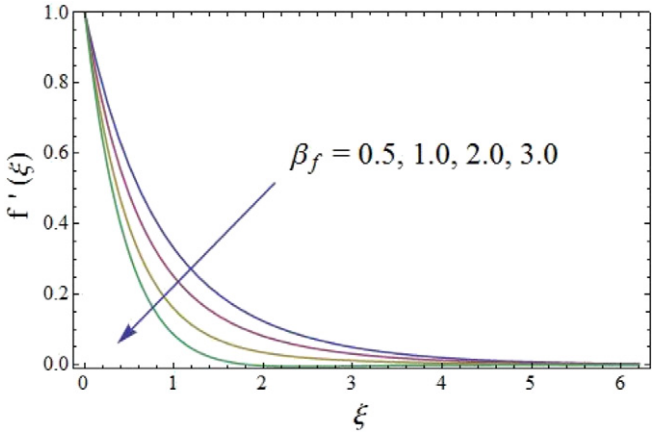

Fig. 3. Impact of parameter β_f on axial velocity.

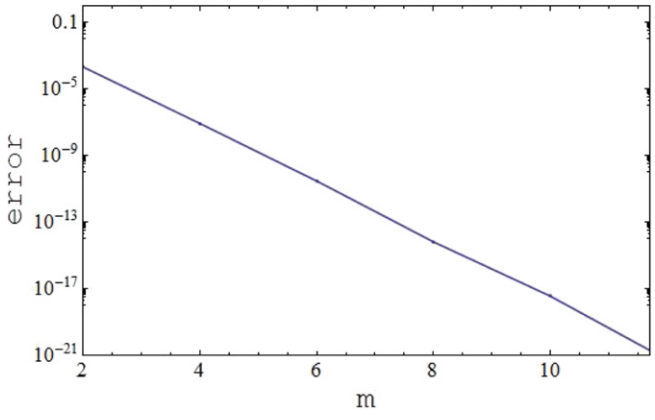

Fig. 2. Shows the error decay for the 10th.*orderapproximation*.

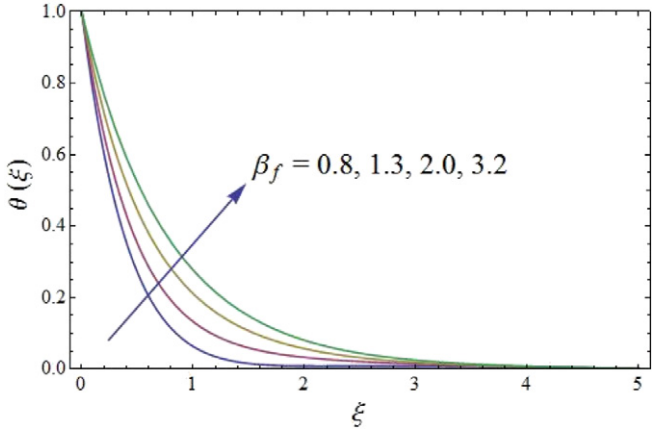

Fig. 4. Impact of parameter β_f on temperature field.

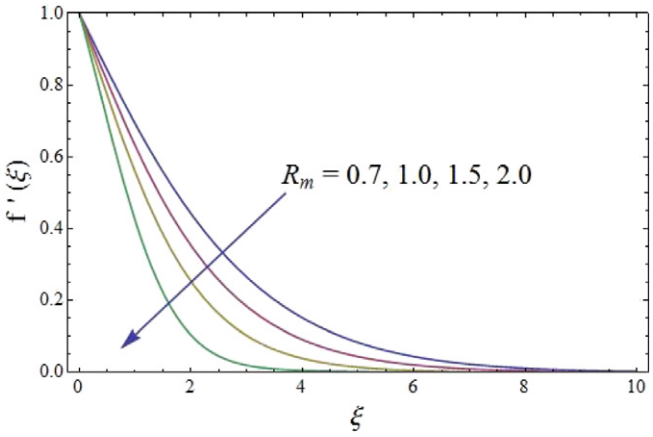

Fig. 5. Influence of parameter R_m on axial velocity.

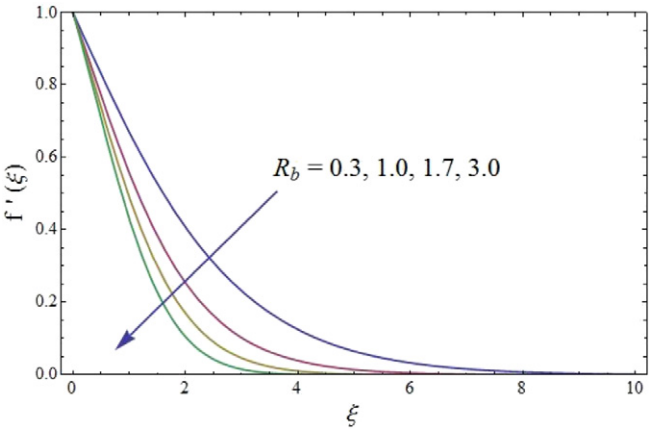

Fig. 8. Effect of parameter R_b on axial velocity.

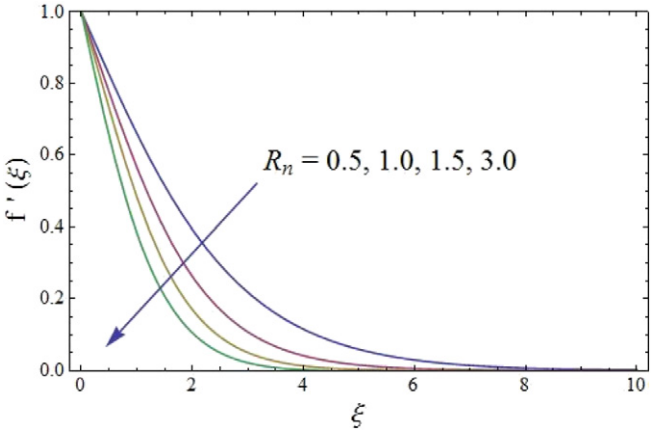

Fig. 6. Influence of parameter R_n on axial velocity.

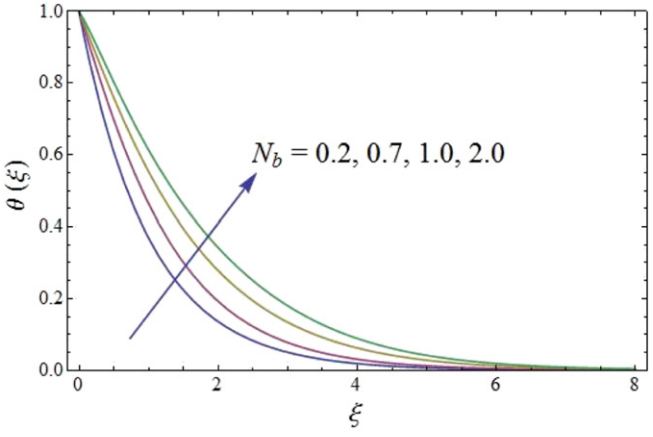

Fig. 9. Consequence of parameter N_b on temperature field.

The influence of parameters N_b (Brownian motion) and N_t (thermophoresis) on the ferromagnetic nanofluid bioconvection flow are carried out in Figs. 9 and 10. The Brownian motion parameter N_b is proportional to the concentration gradient, whereas, thermophoresis parameter N_t is relative to the temperature gradient, giving variation to these parameters results in the enhancement of thermal energy, which is responsible for the increase in temperature field shown in Figs. 9 and 10. The behavior of parameter Pr (Prandtl number) on temperature field is depicted in Fig. 11. It is designated that enlarging the values of parameter (Prandtl number) leads to reduce the thermal conductivity of the fluid, which declines the temperature field shown in Fig. 11.

The impact of parameter L_b (bioconvection Lewis number) on bioconvection ferromagnetic nanofluid flow. Fig. 12 is visualized to depicts the impacts of L_b (bioconvection Lewis number) on the bioconvection ferromagnetic nanofluid flow. An increase in L_b (bioconvection Lewis number) leads to decline the diffusion coefficient of gyrotactic microorganisms, as a result of the density of the motile microorganisms decreases, as depicted in Fig. 12.

5.1. Comparison of viscous and ferromagnetic nanofluids

In the present section, various attempts have been made in such way to analyze the impacts of density of motile microorganisms and magnetic dipole on the flow of ferrofluid. Initially, viscous fluid in absence of magnetic dipole and gyrotactic microorganisms i.e., $R_b = 0$, is incorporated, secondly viscous fluid in absence of magnetic dipole and in presence

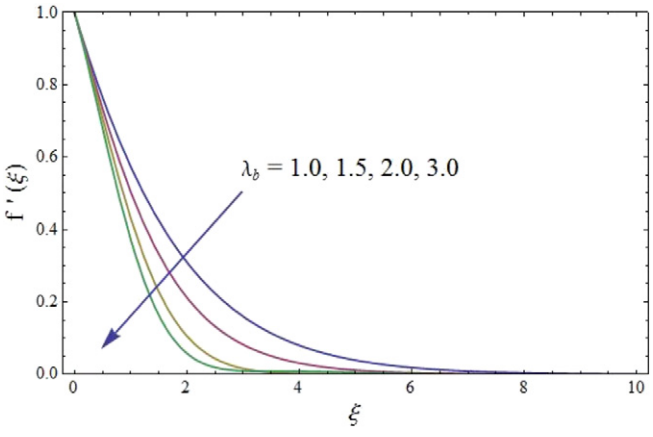

Fig. 7. Impact of parameter λ_b on axial velocity.

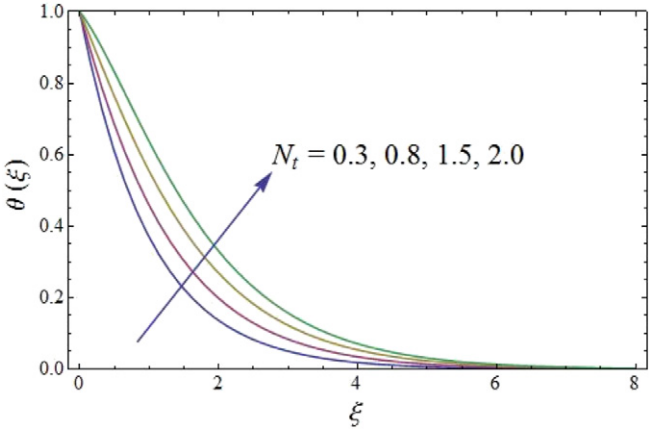

Fig. 10. Influence of parameter N_t on temperature field.

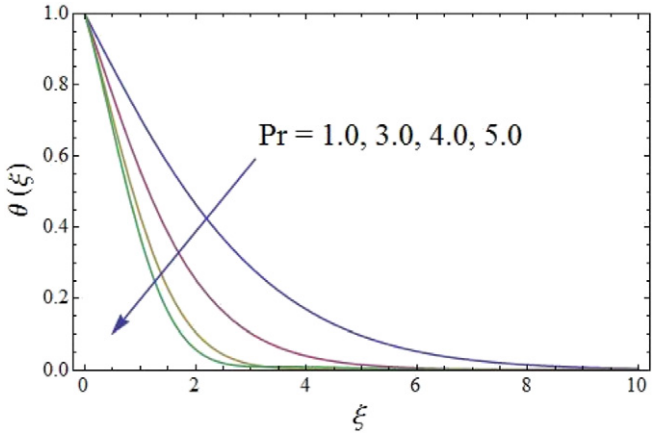

Fig. 11. Consequence of *Pr* on temperature field.

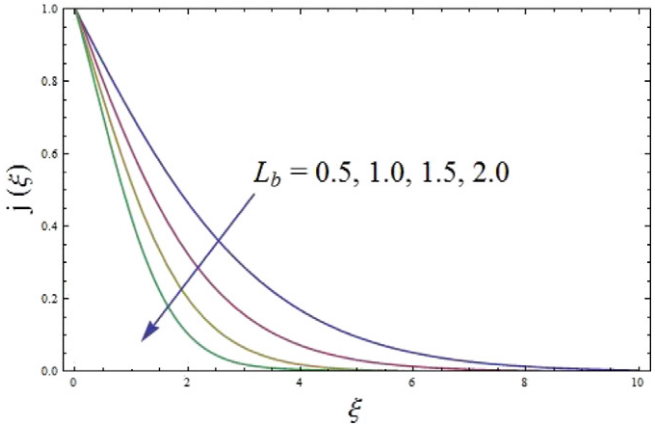

Fig. 12. Impact of parameter L_b on density of motile microorganisms.

of gyrotactic microorganisms i.e., $R_b \neq 0$, is taken, thirdly ferromagnetic nanofluid in absence of magnetic dipole and gyrotactic microorganisms i.e., $R_b = 0$, is considered, and finally ferromagnetic nanofluid in presence of magnetic dipole and gyrotactic microorganisms i.e., $R_b \neq 0$, has been made. The above analysis is plotted in Figs. 13–16. The lowest axial velocity is observed for ferromagnetic nanofluid in presence of gyrotactic microorganisms, i.e., $R_b \neq 0$, whereas the highest axial velocity is depicted for the viscous fluid in absence of motile microorganisms, i.e., $R_b = 0$ as shown in Fig. 13. The highest temperature field is obtained for viscous fluid in absence of motile microorganisms, i.e., $R_b = 0$, whereas the lowest temperature profile is characterized for ferromagnetic nanofluid in presence of gyrotactic microorganisms, $R_b \neq 0$, as shown in Fig. 14. Fig. 15 characterizes that concentration distribution is higher for ferromagnetic nanofluid when the gyrotactic microorganisms

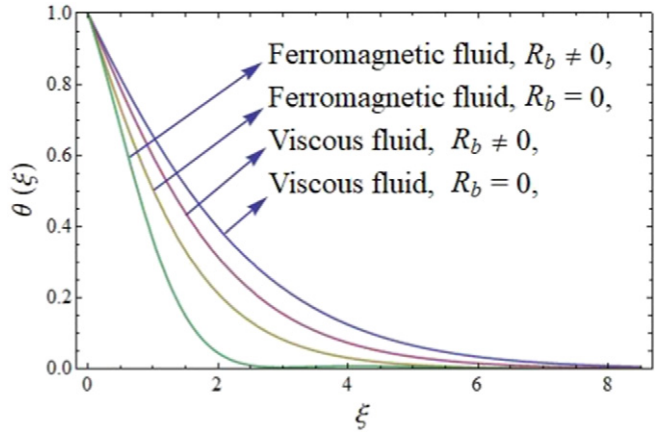

Fig. 14. Influence of sundry parameters on temperature field.

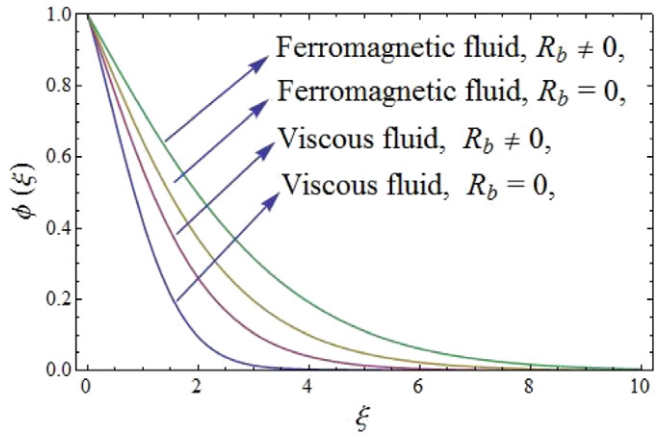

Fig. 15. Effect of sundry parameters on concentration field.

are there, i.e., $R_b \neq 0$, whereas the lower concentration field is depicted for viscous fluid when there is no motile microorganisms, i.e., $R_b = 0$. In Fig. 16, It is determined that the density of motile microorganisms is maximum in ferromagnetic nanofluid in presence of magnetic dipole and the gyrotactic microorganisms, i.e., $R_b \neq 0$, whereas the lowest density of motile microorganisms is depicted for viscous fluid in absence of magnetic dipole and gyrotactic microorganisms, i.e., $R_b = 0$. These graphical results depict that the presence of gyrotactic microorganisms, i.e., $R_b \neq 0$, in the flow of ferromagnetic fluid play an important role and leads to a more realistic and physical situation.

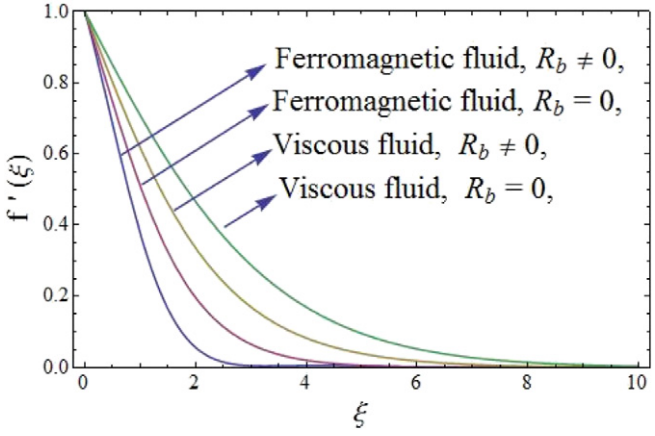

Fig. 13. Effect of sundry parameters on axial velocity.

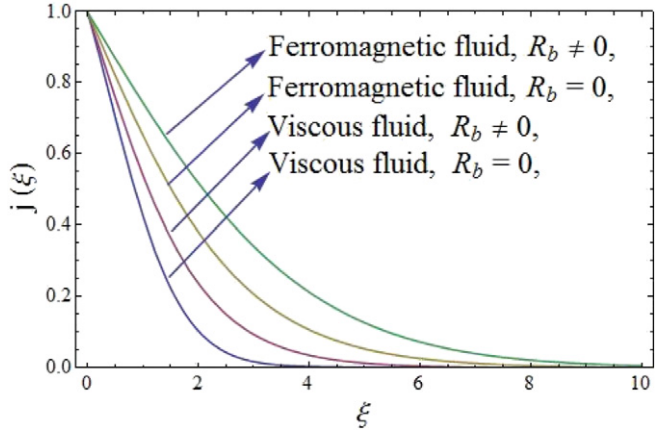

Fig. 16. Influence of sundry parameters on motile microorganisms field.

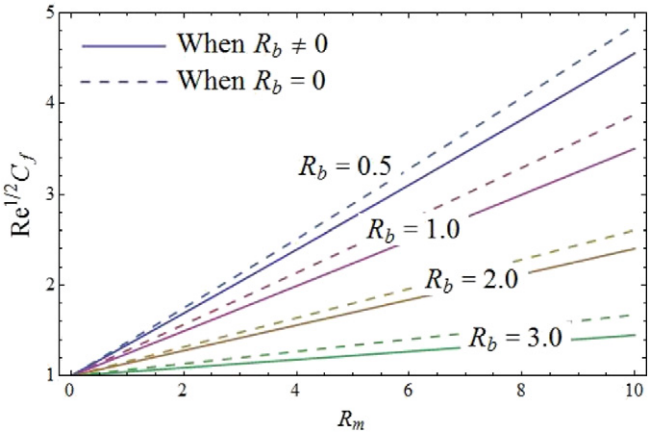

Fig. 17. Wall shear stress versus basic-density Rayleigh number.

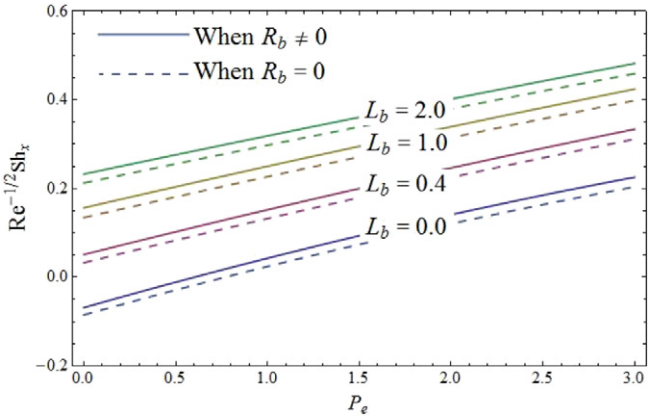

Fig. 19. Sherwood number versus bioconvection Peclet number P_e.

5.2. Parameters of engineering interest

In the present analysis we are interested in, reduce the skin friction, enhance the heat transfer rate, mass transfer rate, and density of motile microorganism as will. The decline in drag friction, enhancement in rate of cooling or heating, enhancement in gradient of nano concentration, and an increase in the density of motile microorganisms are applicable in the advanced technological processes. Thus the present analysis is carried out in presence and in absence of gyrotactic microorganisms i.e., $R_b \neq 0$ and $R_b = 0$ respectively. To get these results, various attempts have been made about the reduction of drag forces or skin friction, and enhancement of heat and mass transfer rates, which are shown in Figs. 17–20. The numerical equations for friction drag, local Nusselt number, local Sherwood number, and the motile microorganisms density are introduced in Eqs. (23)–(25). Fig. 17 characterizes the influence of R_m (basic-density Rayleigh number) on wall shear stress. It is scrutinized that variation in Pr (Prandtl number) in presence of magnetic dipole leads to decline the friction drag. The heat transfer rate via Pr (Prandtl number) is shown in Fig. 18. It is analyzed that the presence of R_b (bioconvection Rayleigh number) results in fast enhancement of heat transfer rate for larger values of λ_b (thermal Rayleigh number). Fig. 19 depicts the impacts of P_e (bioconvection Peclet number) on the Sherwood number. It is designated that larger values of P_e (bioconvection Peclet number) results in the enhancement of concentration gradient at the surface. The effect of L_b (bioconvection Lewis number) on the local density of motile microorganism are depicted in Fig. 20. It is demonstrated that an increment in L_b (bioconvection Lewis number) results in the enhancement of local density of motile microorganism. The drag friction $\frac{1}{2}\mathrm{Re}^{1/2}C_f$ for noticeable values of R_b, R_m, and λ_b are characterized and analyzed in Table 3. Table 4 shows the comparison of Nusselt number for different values of Pr is characterized by means of numerical solution based on BVPh2—midpoint method and analytic solution based on optimal HAM. Table 5 describes the comparison of Sherwood number for different values of R_m, R_b and λ_b. Comparison of motile microorganisms density for several values of R_m, λ_b, and R_b are incorporated in Table 6.

6. Concluding remarks

The analysis concentrates on the evaluation of drag friction, heat transfer rate, mass transfer at the surface, and motile microorganisms density at the surface in the suspension of motile microorganisms. The analysis is carried out in the presence of Curie temperature and magnetic dipole. The aim of the present analysis is to reduce the drag friction and to enhance the heat transfer rate, Sherwood number, local density of motile microorganism. The displayed investigation prompts the accompanying conclusion.

- An enhancement in R_m, β_f, R_n, λ_b, and R_b results in the reduction of the axial velocity.
- The temperature field enhances for higher values of β_f, N_b, and N_t, whereas reduction take place for increasing values of Pr.
- The motile microorganism density reduces with an increase in L_b.
- The lowest axial velocity is observed for the suspension of motile microorganisms in the presence of gyrotactic microorganisms and magnetic dipole, whereas the highest axial velocity is depicted for the viscous fluid in absence of motile microorganisms and magnetic dipole.
- The highest temperature field is obtained for viscous fluid in absence of motile microorganisms and magnetic dipole, whereas the lowest temperature profile is characterized for the motile microorganisms in presence of magnetic dipole and gyrotactic microorganisms.
- Concentration distribution is higher for ferromagnetic nanofluid when the gyrotactic microorganisms and magnetic dipole is present, whereas the lower concentration field is depicted for viscous fluid when there is no motile microorganisms and magnetic dipole.
- The density of motile microorganisms is maximum in ferromagnetic

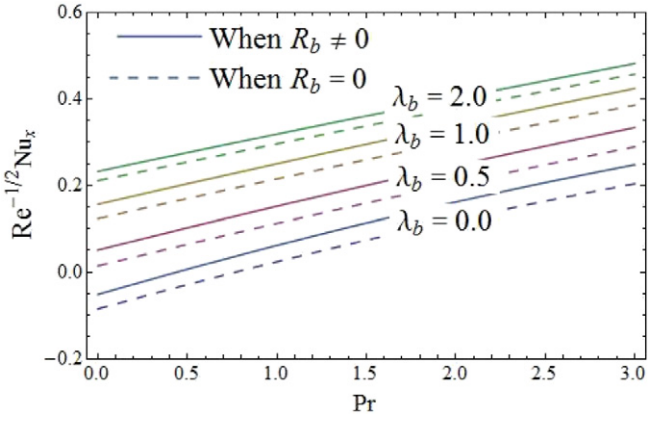

Fig. 18. Heat transfer rate versus *Pr* Prandtl number.

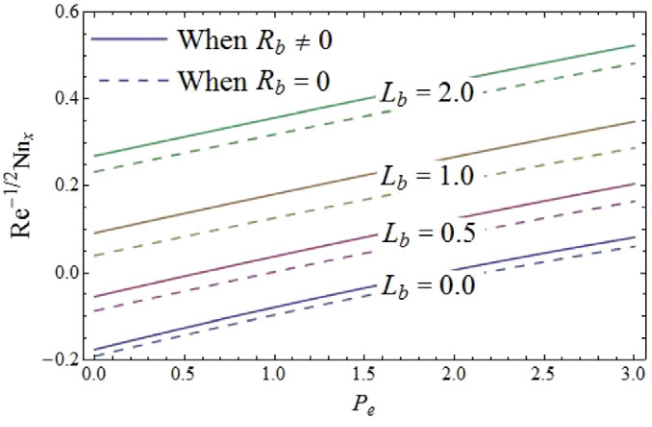

Fig. 20. Motile microorganisms density versus bioconvection Peclet number P_e.

Table 3

The drag friction $\frac{1}{2}\mathrm{Re}\,C_f\,1/2$ for noticeable values of R_b, R_m, and λ_b are characterized and analyzed by means of numerical solution based on BVPh2—midpoint method and analytic solution based on optimal HAM.

$R_b \neq 0$			OHAM results	BVPh2 – Mid point
R_m	R_n	λ_b	$\frac{1}{2}\mathrm{Re}_x^{1/2} C_f$	$\frac{1}{2}\mathrm{Re}_x^{1/2} C_f$
1.0	1.2	1.0	0.79302	0.793023
1.5			0.95105	0.951027
2.0			1.00817	1.008213
1.0	1.2	1.0	0.79302	0.793023
	2.0		1.33001	1.330215
	3.0		1.51810	1.518121
1.0	1.2	1.0	0.79302	0.793023
		1.5	0.76051	0.760569
		2.0	0.79013	0.790157

Table 4

Comparison of Nusselt number for different values of Pr is characterized by means of numerical solution based on BVPh2—midpoint method and analytic solution based on optimal HAM.

Pr	Rashidi [24]	OHAM results	BVPh2 – Mid point
		$\mathrm{Re}^{-1/2} Nu_x$	$\mathrm{Re}_x^{-1/2} N u_x$
0.72	0.808631	0.808581	0.808639
1.0	1.000000	1.000021	1.000021
3.0	1.923682	1.923485	1.923485
5.0	– – –	1.003309	1.003309
7.0	– – –	1.362420	1.362420
9.0	– – –	– – –	1.421430

Table 5

Comparison of Sherwood number for different values of R_m, R_b and λ_b are analyzed by means of analytic solution based on optimal HAM and numerical solution based on BVPh2—midpoint method.

$R_b \neq 0$			OHAM results	BVPh2 – Midpoint
R_m	R_n	λ_b	$\mathrm{Re}^{-1/2} Sh_x$	$\mathrm{Re}^{-1/2} Sh_x$
1.0	1.2	1.0	1.360831	1.360847
1.5			1.009382	1.009360
2.0			0.906220	0.906204
1.0	1.2	1.0	1.360831	1.360847
	2.0		0.994018	0.994076
	3.0		0.872091	0.872043
1.0	1.2	1.0	1.360831	1.360847
		1.5	0.950291	0.950252
		2.0	0.851087	0.851064

Table 6

Comparison of motile microorganisms density for several values of R_m, λ_b, and R_b are incorporated by means of BVPh2—midpoint method and optimal HAM.

$R_b \neq 0$			OHAM results	BVPh2 – Midpoint
R_m	R_n	λ_b	$\mathrm{Re}^{-1/2} Nn_x$	$\mathrm{Re}^{-1/2} Nn_x$
1.0	1.2	1.0	0.79302	0.793023
1.5			0.95105	0.951027
2.0			1.00817	1.008213
1.0	1.2	1.0	0.79302	0.793023
	2.0		1.33001	1.330215
	3.0		1.51810	1.518121
1.0	1.2	1.0	0.79302	0.793023
		1.5	0.76051	0.760569
		2.0	0.79013	0.790157

nanofluid in presence of magnetic dipole and the gyrotactic microorganisms, whereas the lowest density of motile microorganisms is depicted for viscous fluid in absence of magnetic dipole and gyrotactic microorganisms.

- The variation in R_m (basic−density Rayleigh number) in presence of magnetic dipole leads to decline the friction drag.
- The heat transfer rate enhances for increasing values of parameter β_f (ferrohydrodynamic interaction).
- The larger values of P_e (bioconvection Peclet number) results in the enhancement of concentration gradient at the surface.
- An increment in L_b (bioconvection Lewis number) results in the enhancement of local density of motile microorganism.

Acknowledgment

The author(s) disclosed receipt of the following financial support for the research, authorship, and/or publication of this article: This paper was funded by the Higher Education Commission, Pakistan (HEC), under grant no. 6170/Federal/NRPU/R&D/HEC/2016.

Author(s) would like to acknowledge and express their gratitude also to the Higher Education Commission, Islamabad, Pakistan, for the award of scholarship under "International Research Support Initiative Program" grant No: I-8/HEC/HRD/2018/8972, PIN: IRSIP 41 PSc 28, for Texas A&M University, USA.

References

[1] M.M. Hopkins, L.J. Fauci, A computational model of the collective fluid dynamics of motile micro-organisms, J. Fluid Mech. 455 (2002) 149–174.
[2] A.M. Roberts, Geotaxis in motile micro-organisms, J. Exp. Biol. 3 (53) (1970) 687–699.
[3] A.V. Kuznetsov, The onset of bioconvection in a suspension of gyrotactic microorganisms in a fluid layer of finite depth heated from below, Int. Commun. Heat Mass Transf. 5 (2005) 574–582.
[4] M.P. Mkhatshwa, F.G. Awad, M. Khumalo, Cross-diffusion effects on unsteady bioconvective flow past a stretching sheet, J. Heat Transf. 3 (2017), 031101.
[5] A. Mahdy, Free convection flow over a vertical flat plate in nanofluid porous media containing gyrotactic microorganisms with prescribed density motile microorganisms flux, Sci. Technol. Aliment. 2 (2017) 91–105.
[6] W.A. Khan, O.D. Makinde, MHD nanofluid bioconvection due to gyrotactic microorganisms over a convectively heat stretching sheet, Int. J. Therm. Sci. 81 (2014) 118–124.
[7] A.V. Kuznetsov, Non-oscillatory and oscillatory nanofluid bio-thermal convection in a horizontal layer of finite depth, Eur. J. Mech. B Fluid 2 (2011) 156–165.
[8] D.A. Nield, A.V. Kuznetsov, The onset of convection in a horizontal nanofluid layer of finite depth, Eur. J. Mech. B Fluid 3 (2010) 217–223.
[9] S. Ghorai, N.A. Hill, Development and stability of gyrotactic plumes in bioconvection, J. Fluid Mech. 400 (1999) 1–31.
[10] T.J. Pedley, N.A. Hill, J.O. Kessler, The growth of bioconvection patterns in a uniform suspension of gyrotactic micro-organisms, J. Fluid Mech. 195 (1988) 223–237.
[11] C.S.K. Raju, M.M. Hoque, T. Sivasankar, Radiative flow of Casson fluid over a moving wedge filled with gyrotactic microorganisms, Adv. Powder Technol. 2 (2017) 575–583.
[12] A.J. Chamkha, A.M. Rashad, P.K. Kameswaran, M.M.M. Abdou, Radiation effects on natural bioconvection flow of a nanofluid containing gyrotactic microorganisms past a vertical plate with streamwise temperature variation, J. Nanofluids 3 (2017) 587–595.
[13] D.A. Nield, A.V. Kuznetsov, The onset of convection in a horizontal nanofluid layer of finite depth, Eur. J. Mech. B Fluid 3 (2010) 217–223.
[14] D.A. Nield, A.V. Kuznetsov, The onset of bio-thermal convection in a suspension of gyrotactic microorganisms in a fluid layer: oscillatory convection, Int. J. Therm. Sci. 10 (2006) 990–997.
[15] S. Mosayebidorcheh, M.A. Tahavori, T. Mosayebidorcheh, D.D. Ganji, Analysis of nano-bioconvection flow containing both nanoparticles and gyrotactic microorganisms in a horizontal channel using modified least square method (MLSM), J. Mol. Liq. 227 (2017) 356–365.
[16] T. Abe, S. Nakamura, S. Kudo, Bioconvection induced by bacterial chemotaxis in a capillary assay, Biochem. Biophys. Res. Commun. 1 (2017) 277–282.
[17] S. Xun, J. Zhao, L. Zheng, X. Zhang, Bioconvection in rotating system immersed in nanofluid with temperature dependent viscosity and thermal conductivity, Int. J. Heat Mass Transf. 111 (2017) 1001–1006.
[18] M. Arruebo, R.F. Pacheco, M.R. Ibarra, J. Santamarí a, Magnetic nanoparticles for drug delivery, Nano Today 3 (2) (2007) 22–32.
[19] J.L. Neuringer, Some viscous flows of a saturated ferro− fluid under the combined influence of thermal and magnetic field gradients, Int. J. Non−Linear Mech. 2 (1966) 123–137.
[20] N. Sivakumar, P. Durga Prasad, C.S.K. Raju, S.V.K. Varma, S.A. Shehzad, Partial slip and dissipation on MHD radiative ferro-fluid over a non-linear permeable convectively heated stretching sheet, Results in Physics 7 (2017) 1940–1949, https://doi.org/10.1016/j.rinp.2017.06.016.
[21] L.J. Crane, Flow past a stretching plate, Zeitschrift fu¨r angewandte Mathematik und Physik ZAMP 4 (21) (1970) 645–647.
[22] H.I. Andersson, O.A. Valnes, Flow of a heated ferrofluid over a stretching sheet in the presence of a magnetic dipole, Acta Mech. 1−2 (128) (1998) 39–47.
[23] A. Alsaedi, M.I. Khan, M. Farooq, N. Gull, T. Hayat, Magnetohydrodynamic (MHD) stratified bioconvective flow of nanofluid due to gyrotactic microorganisms, Adv. Powder Technol. 1 (28) (2017) 288–298.
[24] R. Ellahi, M.H. Tariq, M. Hassan, K. Vafai, On boundary layer nano-ferroliquid flow under the influence of low oscillating stretchable rotating disk, J. Mol. Liq. 229 (2017) 339–345.
[25] N. Ijaz, A. Zeeshan, M.M. Bhatti, R. Ellahi, Analytical study on liquid-solid particles interaction in the presence of heat and mass transfer through a wavy channel, J. Mol. Liq. 250 (2018) 80–87.
[26] R. Ellahi, A. Zeeshan, N. Shehzad, S.Z. Alamri, Structural impact of Kerosene-Al_2O_3 nanoliquid on MHD Poiseuille flow with variable thermal conductivity: application of cooling process, J. Mol. Liq. 264 (2018) 607–615.
[27] S.Z. Alamri, R. Ellahi, N. Shehzad, A. Zeeshan, Convective radiative plane Poiseuille flow of nanofluid through porous medium with slip: an application of Stefan blowing, J. Mol. Liq. 273 (2019) 292–304.
[28] A. Sohail, M. Fatima, R. Ellahi, K.B. Akram, A videographic assessment of Ferrofluid during magnetic drug targeting: an application of artificial intelligence in nanomedicine, J. Mol. Liq. 285 (2019) 47–57.
[29] A. Zeeshan, F. Hussain, R. Ellahi, K. Vafai, A study of gravitational and magnetic effects on coupled stress bi-phase liquid suspended with crystal and Hafnium particles down in steep channel, J. Mol. Liq. 286 (2019) 110898.
[30] K.M. Shirvan, M. Mamourian, S. Mirzakhanlari, R. Ellahi, Two phase simulation and sensitivity analysis of effective parameters on combined heat transfer and pressure drop in a solar heat exchanger filled with nanofluid by RSM, J. Mol. Liq. 220 (2016) 888–901.
[31] M. Sheikholeslami, M.T. Mustafa, D.D. Ganji, Effect of Lorentz forces on forced-convection nanofluid flow over a stretched surface, Particuology 26 (2016) 108–113.
[32] S. Ahmad, S. Nadeem, N. Muhammad, Boundary layer flow over a curved surface imbedded in porous medium, Commun. Theor. Phys. 3 (71) (2019) 344.
[33] N. Muhammad, S. Nadeem, M.T. Mustafa, Hybrid isothermal model for the ferrohydrodynamic chemically reactive species, Commun. Theor. Phys. 4 (71) (2019) 384.
[34] N. Muhammad, S. Nadeem, A. Issakhov, Finite volume method for mixed convection flow of Ag-ethylene glycol nanofluid flow in a cavity having thin central heater, Phys. A Stat. Mech. Appl. 537 (2019) 122738.
[35] N. Muhammad, S. Nadeem, T. Mustafa, Heat transport phenomenon in the ferromagnetic fluid over a stretching sheet with thermal stratification, Results in Physics 12 (2016) 027.
[36] S. Liao, Beyond Perturbation: Introduction to Homotopy Analysis Method, Chapman and Hall, CRC Press, Boca Raton, 2003.
[37] S. Liao, Advances in the Homotopy Analysis Method, World Scientific (2013).